Photochemical & Photobiological Sciences

ROYAL SOCIETY OF CHEMISTRY

PAPER

Photochemistry of hexachloroosmate(IV) in ethanol†

Evgeni M. Glebov, *[a,b] Svetlana G. Matveeva, [a] Ivan P. Pozdnyakov,[a,b] Vjacheslav P. Grivin,[a,b] Victor F. Plyusnin,[a,b] Danila B. Vasilchenko, [c,b] Tamara E. Romanova,[c,b] Alexei A. Melnikov,[d,e] Sergey V. Chekalin[d] and Roman G. Fedunov[a]

Received 15th July 2020,
Accepted 30th September 2020

DOI: 10.1039/d0pp00244e

rsc.li/pps

The photochemistry of the $Os^{IV}Cl_6^{2-}$ complex in ethanol was studied by means of stationary photolysis, nanosecond laser flash photolysis, ultrafast pump–probe spectroscopy and quantum chemistry. The direction of the photochemical process was found to be wavelength-dependent. Irradiation in the region of the d–d and LMCT bands results in the photosolvation (with the wavelength-dependent quantum yield) and photoreduction of Os(IV) to Os(III), correspondingly. The characteristic time of photosolvation is *ca.* 40 ps. Photoreduction occurs in the micro- and millisecond time domains *via* several Os(III) intermediates. The nature of intermediates and the possible mechanisms of photoreduction are discussed. We believe that the lability of the photochemically produced Os(IV) and Os(III) intermediates determines the synthetic potential of $Os^{IV}Cl_6^{2-}$ photochemistry.

1. Introduction

The photochemistry of osmium complexes is potentially interesting because the electronic configuration of an osmium atom ($5d^6 6s^2$) leads to the existence of oxidation states from +8 to −2, among which compounds with valences VIII, VI and IV are the most stable.[1] Several potential fields of application of osmium complexes are based on their photophysics and photochemistry. Complexes with organic ligands and organometallic compounds have been applied for the development of luminescent sensors, dye-sensitized solar cells and electroluminescent devices (see ref. 2 and references therein) as well as for diarylethene-based optical switches (see ref. 3 and references therein). Another field of application of the osmium complex photochemistry is photocatalysis.[4–6] Rather simple complexes, like $Os_3(CO)_{12}$ [4] and $Os^{IV}Cl_6^{2-}$,[6] are used as photocatalysts. For successful application, the knowledge of the mechanistic photochemistry of osmium complexes is necessary.

The $Os^{IV}Cl_6^{2-}$ complex, as one of the simplest, can be considered as a model compound allowing one to follow all the stages of photochemical transformations, from the absorption of light to the formation of final products. Irradiation of this complex in water,[7,8] methanol,[8] acetonitrile and pyridine[7] resulted in photosolvation, while irradiation in chloroform gave rise to photooxidation of Os(IV) to Os(V).[6]

Recently we have performed a case study of the $Os^{IV}Cl_6^{2-}$ photochemistry in aqueous solutions.[9] The primary stage of photolysis was found to be photoaquation followed by acid dissociation of $Os^{IV}Cl_5(H_2O)^-$ to $Os^{IV}Cl_5(OH)^{2-}$. The process is completed in the picosecond time domain. The photochemical reaction occurs *via* the formation and decay of one intermediate (key intermediate, KI) with the characteristic lifetime being as small as 23 ps. Quantum chemical calculations of the electronic absorption spectra of the possible structures were performed, and the KI was identified as the pentacoordinated $Os^{IV}Cl_5^-$ complex with a square pyramidal coordination geometry.[10] The multiplicity of the KI can be either triplet or quintet: both possibilities do not contradict with the results of calculations. The adequacy of the KI interpretation was supported by similar calculations performed for the UV spectra of the photoaquation products – $Os^{IV}Cl_5(H_2O)^-$ and $Os^{IV}Cl_5(OH)^{2-}$.[11] The $Os^{IV}Br_6^{2-}$ complex, which is isoelectronic

[a]*V.V. Voevodsky Institute of Chemical Kinetics and Combustion, 3 Institutskaya Str., 630090 Novosibirsk, Russian Federation. E-mail: glebov@kinetics.nsc.ru; Fax: +7383 3307350; Tel: +7 383 3309150*

[b]*Novosibirsk State University, 2 Pirogova Str., 630090 Novosibirsk, Russian Federation*

[c]*A.V. Nikolaev Institute of Inorganic Chemistry, 3 Lavrentyev Ave., 630090 Novosibirsk, Russian Federation. E-mail: vasilchenko@niic.nsc.ru*

[d]*Institute of Spectroscopy, Russian Academy of Sciences, 5 Fizicheskaya Str., 119333 Troitsk, Moscow, Russian Federation. E-mail: melnikov@isan.troitsk.ru*

[e]*Faculty of Physics, National Research University Higher School of Economics, 20 Myasnitskaya Str., 101000 Moscow, Russian Federation*

† Electronic supplementary information (ESI) available: Detailed information on the geometric and electronic structures of the complexes under consideration, additional information concerning its stationary and laser flash photolysis and the results of quantum chemical calculations. See DOI: 10.1039/d0pp00244e

to $Os^{IV}Cl_6^{2-}$, undergoes photosolvation in aqueous and methanol solutions occurring in the picosecond time domain *via* the formation of the $^3Os^{IV}Br_5^-$ intermediate.[12,13] Therefore, the photochemical behaviour of $Os^{IV}Cl_6^{2-}$ and $Os^{IV}Br_6^{2-}$ is identical.

In this work we study the photochemistry of $Os^{IV}Cl_6^{2-}$ in ethanol. The characteristic feature of metal complex photochemistry in alcohols (compared with aqueous solutions) is the possibility of photoreduction *via* electron transfer from the solvent molecule to the light-excited complex. This process was well documented for $PtCl_6^{2-}$ (ref. 14 and 15) and $IrCl_6^{2-}$ (ref. 16 and 17) complexes. Photoreduction was not observed for $Os^{IV}Cl_6^{2-}$ in methanol, but near-UV irradiation of the $Os^{IV}Cl_5(CH_3OH)^-$ complex in deaerated solutions resulted in the reduction of Os(IV) to Os(III).[8] The study was performed in the time range starting from 100 fs, as was previously done for several hexahalide[12,18–23] and pseudohexahalide[24] complexes of platinum metals.

2. Experimental

Solutions of the $Os^{IV}Cl_6^{2-}$ complex were prepared from $Na_2OsCl_6{\cdot}H_2O$ salt purchased from Aldrich or synthesized as described in ref. 25. Spectrophotometric-grade ethanol was used for the sample preparation. If necessary, samples were deaerated by bubbling with argon.

A Varian Cary 50 spectrophotometer (Varian Inc.) was used for recording UV absorption spectra. Steady-state photolysis was performed by the radiation of a high-pressure mercury lamp with a set of glass filters for separating necessary wavelengths. In several experiments, an excimer XeCl lamp (excilamp) was used as a quasicontinuous source of radiation at 308 nm (half width of light pulse, 5 nm; pulse duration, 1 μs; frequency, 200 kHz; incident light flux, 8×10^{15} photons·cm^{-2} s^{-1}).[26]

The concentration of Cl^- was measured using a Metrohm 883 Baisc IC Plus liquid chromatograph (Metrohm, Switzerland) with a conductometric detector equipped with a 20 μL sample loop, a Metrosep A Supp 5 150/4.0 column and a suppressor module. Mobile phase: 3.2×10^{-3} M Na_2CO_3, 1.0×10^{-3} M $NaHCO_3$; flow rate: 0.7 L min^{-1}. The calibration was done in the concentration range of 0.1–100 ppm of Cl^-.

Nanosecond laser flash photolysis experiments were performed using excitation by irradiation with a Nd:YAG laser (Lotis TII, Belarus, 355 nm, 5 ns pulse duration, up to 10 mJ per pulse energy). Probing typically was performed by irradiation with a Xe lamp DKSh-150 (Russia) exploited in the pulsed regime. In the millisecond time domain, LEDs were used for probing. The setup is described in detail in ref. 27.

A light power meter SOLO 2 (Gentec, Canada) was used to measure the radiation intensity for the quantum yield calculations in stationary experiments and to control the laser pulse energy in the course of laser flash photolysis experiments.

Ultrafast pump–probe spectroscopy was used to study transient absorption in the picosecond time domain. The experimental setup is described in detail in ref. 28. The samples were excited with ~60 fs pulses (energy, *ca.* 1 μJ, pulse repetition rate, 1 kHz) at ~400 nm (second harmonic of a Ti:sapphire generator-amplifier system, CDP Ltd, Moscow, Russia). The solutions with a total volume of 20 mL were pumped through a 1 mm quartz cell at room temperature to provide uniform irradiation and avoid possible degradation due to photochemical reactions. To record a single time-resolved spectrum, 200 pulses were used. Each kinetic curve contained 110 points (60 points with a 100 fs step, 20 points with a 500 fs step, and 30 points with a 3 ps step). ExciPro program (CDP System Corporation) was used for corrections of the group velocity dispersion. The corrected experimental data were globally fitted using several exponential functions. The PyGSpec program[29] was used for global fitting.

Quantum chemical calculations of the geometry and energy of $Os^{IV}Cl_6^{2-}$, $Os^{IV}Cl_5(EtOH)^-$, $Os^{IV}Cl_5^-$, $Os^{III}Cl_4^-$, $Os^{III}Cl_5^{2-}$ and $Os^{IV}Cl_5(EtO)^{2-}$ were performed using the B3LYP density functional method[30,31] with the DEF2-TZVP/C basic set[32] (and DEF2-ECP for Os[33]). Optimization of all the geometric parameters was performed using the gradient method for the lowest electronic excited state of the given multiplicity (singlet, triplet and quintet). Calculations were performed within a single molecule approximation both in the gas phase and in ethanol as a solvent. The solvent effect was taken into account in the framework of the polarizable continuum model (LR-CPCM).[34–36] The TD-DFT method was used to calculate the electronic absorption spectra. Hessian and thermochemical parameters of all the mentioned compounds were calculated. There were no optimized structures represented by negative frequencies. ORCA (4.1.1, 4.2.0, 4.2.1) software packages[37] were used for calculations. ChemCraft software[38] was used for the visualization of computations.

3. Results and discussion

3.1. Steady-state photolysis of $Os^{IV}Cl_6^{2-}$

$Os^{IV}Cl_6^{2-}$ is a low spin complex with the $5d^4$ electronic configuration. In the literature, O_h symmetry is typically used for the description of the $Os^{IV}Cl_6^{2-}$ spectroscopy[39,40] in spite of the small Jahn–Teller distortion to lower symmetry. In the framework of the crystal field approach with the octahedral symmetry, the ground state is triplet ($^3T_{1g}$ [40]). For clarification, Fig. S1 of the ESI† shows the approximate structure of the orbitals.

The UV spectrum of $Os^{IV}Cl_6^{2-}$ in ethanol (curve 1 in Fig. 1) is similar to that in aqueous solutions.[9] A shoulder in the region of 405–418 nm (molar absorption coefficient $\varepsilon \sim 900$ M^{-1} cm^{-1}) was assigned by Jørgensen to an LMCT transition.[39,41] This band corresponds to the $\pi_{Cl}(t_{1g}) \rightarrow Os(t_{2g})$ promotion. The LMCT bands in the region of 320–375 nm appeared as a doublet (λ_{max} = 341 and 347 nm, ε = 7090 and 7140 M^{-1} cm^{-1}, correspondingly) and a single band with a maximum at 372 nm and ε = 6700 M^{-1} cm^{-1}. These bands correspond to $\pi_{Cl}(t_{2u}) \rightarrow Os(t_{2g})$ and $(\pi + \sigma)_{Cl}(t_{1u}) \rightarrow Os(t_{2g})$ pro-

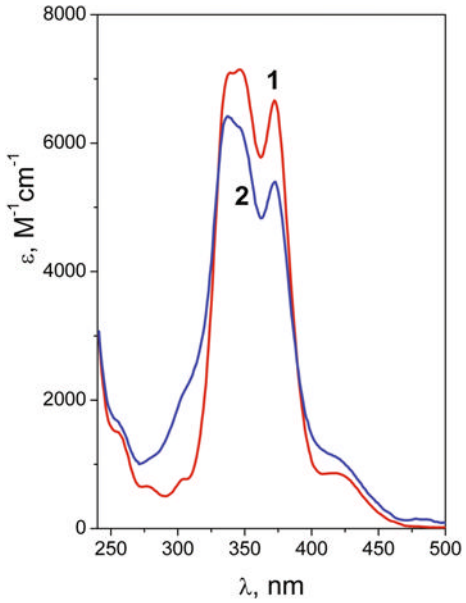

Fig. 1 Electronic absorption spectra of the complexes $Os^{IV}Cl_6^{2-}$ (1) and $Os^{IV}Cl_5(C_2H_5OH)^-$ (2, see text) in ethanol solution.

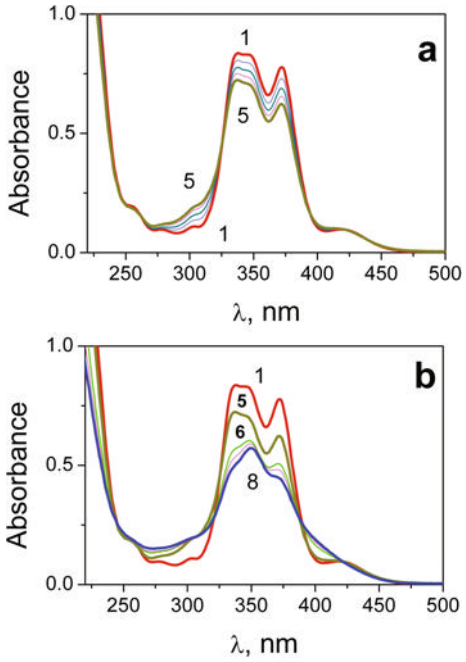

Fig. 2 Changes in the UV absorption spectrum caused by irradiation (313 nm, 1 cm quartz cell) of $Os^{IV}Cl_6^{2-}$ (1.2×10^{-4} M) in air-saturated ethanol. Panels a and b represent different stages of the process. Curves 1–8 correspond to 0, 15, 30, 45, 60, 184, 234, and 300 min of irradiation.

motions.[39] The most intense ($\varepsilon \approx 20\,000$ M^{-1} cm^{-1}) LMCT band has the maximum in the region of 210 nm (not shown in Fig. 1); it is assigned to the $\pi_{Cl} \rightarrow Os(e_g)$ promotion.[40] In the region of 250–310 nm, the d–d and LMCT bands are partially superimposed.[39] $Os^{IV}Cl_6^{2-}$ is rather stable in ethanolic solutions. Different from the case of aqueous solutions,[9] no remarkable thermal reaction was observed in the time interval of 24 h.

The nature of the photochemical processes was found to be wavelength-dependent. The changes in the UV absorption spectrum caused by irradiation at 308 or 313 nm (the region when d–d and LMCT bands are superimposed) are shown in Fig. 2. Irradiation at 405 nm (*i.e.* in the region of the low energy LMCT bands) results in similar spectral changes. Fig. 2a demonstrates the first stage of photolysis, in which the isosbestic points at 262, 326 and 394 nm are conserved. Based on the analogy with the case of $Os^{IV}Cl_6^{2-}$ photolysis in water[7] and methanol,[8] we expected that the first stage would be photosolvation.

$$Os^{IV}Cl_6^{2-} + C_2H_5OH \xrightarrow[\text{d–d band}]{h\nu} Os^{IV}Cl_5(C_2H_5OH)^- + Cl^- \quad (1)$$

This hypothesis was supported by measuring the amount of released Cl^- anions in the course of photolysis. The yield of Cl^- was linear *vs.* irradiation time both for 313 and 405 nm excitation (Fig. 3) in the time range of the conservation of isosbestic points (Fig. 2a). As one can see in Fig. 3, linearity is observed till the almost complete release of one Cl^- anion. It means that photosolvation (1) is exactly the first stage of photolysis, and its quantum yield is sufficiently higher than the quantum yields of the secondary reactions. It allowed us to extract the electronic absorption spectrum of the $Os^{IV}Cl_5(C_2H_5OH)^-$ complex (curve 2 in Fig. 1; an example of raw spectral data is shown in Fig. S2 of the ESI†).

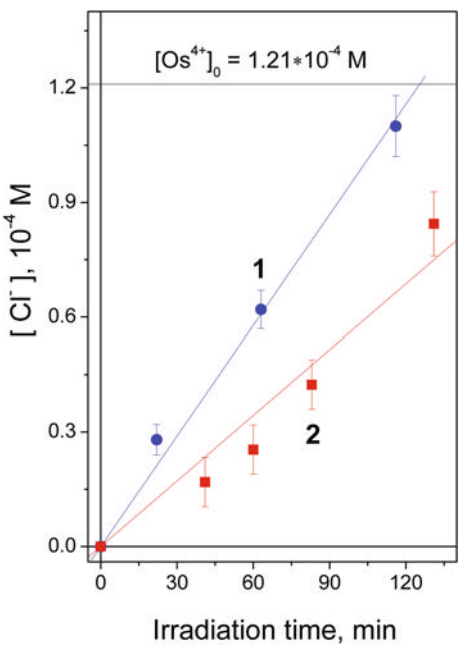

Fig. 3 Changes in the concentration of released Cl^- in the course of $Os^{IV}Cl_6^{2-}$ photolysis in EtOH. Initial concentration 1.21×10^{-4} M, air-saturated solutions. Curves 1 and 2 (experimental points and linear fits) correspond to irradiation at 313 and 405 nm.

The spectrum of $Os^{IV}Cl_5(C_2H_5OH)^-$ differs noticeably from those of the $Os^{IV}Cl_5(H_2O)^-$ and $Os^{IV}Cl_5(OH)^{2-}$ complexes.[9] It contains a doublet (λ_{max} = 337 and 346 nm) and a single band (λ_{max} = 373 nm) corresponding to the $\pi_{Cl}(t_{2u}) \rightarrow Os(t_{2g})$ and $(\pi + \sigma)_{Cl}(t_{1u}) \rightarrow Os(t_{2g})$ promotions, which are close to the same bands in the spectrum of the initial $Os^{IV}Cl_6^{2-}$ complex. The sufficient differences in the spectra of $Os^{IV}Cl_5(C_2H_5OH)^-$ and $Os^{IV}Cl_6^{2-}$ lie in the regions of 275–315 nm and 400–425 nm, where the solvated complex has sufficiently higher absorption.

Knowing the spectrum of the product, we have calculated the quantum yields of photosolvation, which are presented in Table 1. No effect of dissolved oxygen on the quantum yield was observed. For the case of irradiation at 308 nm the quantum yield is moderate, but excitation at 405 nm results in photosolvation with a rather low quantum yield. Therefore, in this case we observe the typical situation for the photochemistry of coordination compounds, when d–d excitation is favorable for the reaction of ligand exchange, while the charge transfer excitation is not.[42] The low-energy LMCT bands in the region of 405 nm demonstrate very poor photochemical activity. This situation is similar to the case of the $IrCl_6^{2-}$ complex, for which the low-energy LMCT bands are not photoactive both in aqueous[43,44] and alcohol[16,17] solutions.

At the second stage of photolysis (Fig. 2b), the band with the maximum at 348 nm is formed. The quantum yield of this stage is roughly five times less than that of the first one. As we will see further, the second stage is more likely the photoreduction of the $Os^{IV}Cl_5(C_2H_5OH)^-$ complex (eqn (2)) than its further photosolvation (eqn (3)).

$$Os^{IV}Cl_5(C_2H_5OH)^- \xrightarrow[C_2H_5OH]{h\nu} Os^{III}Cl_5(C_2H_5OH)^{2-} + {}^{\bullet}C_2H_4OH + H^+ \quad (2)$$

$$Os^{IV}Cl_5(C_2H_5OH)^- \xrightarrow[C_2H_5OH]{h\nu} Os^{IV}Cl_4(C_2H_5OH)_2 + Cl^- \quad (3)$$

Irradiation at 365 nm, which corresponds to the moderate-to-intense LMCT bands caused by $\pi_{Cl}(t_{2u}) \rightarrow Os(t_{2g})$ and $(\pi + \sigma)_{Cl}(t_{1u}) \rightarrow Os(t_{2g})$ promotions,[40] results in a change in the direction of the photochemical process. The photolysis is two-stage again (Fig. 4). In the first stage (Fig. 4a), five isosbestic points at 245, 254, 261, 323 and 390 nm are conserved. The new band with the maximum at 352 nm is formed. Note that the appearance of the spectrum at the end of the first stage (curves 4 and 5 in Fig. 4) resembles that formed at the second stage of the d–d band photolysis (curve 8 in Fig. 2b). We have proposed that the irradiation in the region of the LMCT band results in the outer-sphere electron transfer from the solvent molecule to the light-excited complex, as in the case of $PtCl_6^{2-}$ (ref. 14 and 15) and $IrCl_6^{2-}$ (ref. 16 and 17) alcohol solutions:

$$Os^{IV}Cl_6^{2-} + C_2H_5OH \xrightarrow[\text{LMCT band}]{h\nu} Os^{III}Cl_6^{3-} + {}^{\bullet}C_2H_4OH + H^+ \quad (4)$$

The $Os^{III}Cl_6^{3-}$ complex in aqueous solutions has absorption bands with the maxima at 262 and 282 nm.[39] Therefore, the band with the maximum at 352 nm could not belong to $Os^{III}Cl_6^{3-}$. After the electron transfer (4), there are several possibilities. The first possibility is the successive dissociation of the $Os^{III}Cl_6^{3-}$ intermediate with the formation of penta- and tetracoordinated structures $Os^{III}Cl_5^{2-}$ and $Os^{III}Cl_4^-$ (like in the case of $Pt^{IV}Cl_6^{2-}$ photolysis in methanol[14]).

$$Os^{III}Cl_6^{3-} \rightarrow Os^{III}Cl_5^{2-} + Cl^- \quad (5)$$

$$Os^{III}Cl_5^{2-} \rightarrow Os^{III}Cl_4^- + Cl^- \quad (6)$$

The second possibility is the thermal solvation of $Os^{III}Cl_6^{3-}$ (eqn (7)). In this case, the band at 352 nm belongs to the $Os^{III}Cl_{6-n}(C_2H_5OH)^{(3-n)-}$ complex. Note that for n = 1 the final product is the same as in the case of prolonged photolysis in the d–d band region (eqn (2)).

$$Os^{III}Cl_6^{3-} + nC_2H_5OH \rightarrow Os^{III}Cl_{6-n}(C_2H_5OH)_n^{(3-n)-} + nCl^- \quad (7)$$

The third possibility is the disproportionation of two Os(III) complexes to Os(II) and Os(IV) (eqn (8)). The composition of the

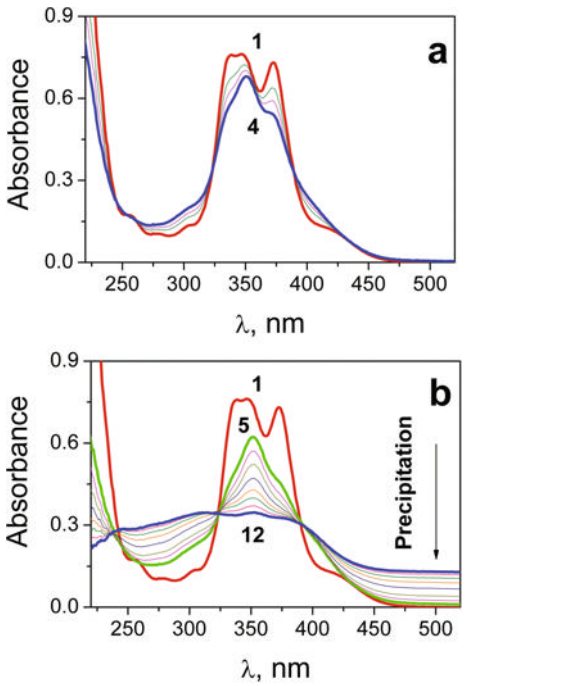

Fig. 4 Changes in the UV absorption spectrum caused by irradiation (365 nm, 1 cm quartz cell) of $Os^{IV}Cl_6^{2-}$ (1.1×10^{-4} M) in air-saturated ethanol. Panels a and b represent different stages of the process. Curves 1–12 correspond to 0, 3, 5, 8, 15, 22, 31, 45, 60, 75, 91, and 111 min of irradiation.

Table 1 Quantum yields of $Os^{IV}Cl_6^{2-}$ photolysis in ethanol

$\varphi^{308\ nm}$	$\varphi^{405\ nm}$	$\varphi^{365\ nm}$ (estimation)
Photosolvation	Photosolvation	Photoreduction
0.15 ± 0.03	$(1.9 \pm 0.3) \times 10^{-3}$	0.03

ligands could be different. In this case, the band at 352 nm belongs to the Os(II) complex.

$$2\mathrm{Os(III)} \rightarrow \mathrm{Os(II)} + \mathrm{Os(IV)} \quad (8)$$

Note that the experiments with the quantification of Cl^- release in the course of photolysis cannot support or rule out the primary process (4). The information on the nature of the photochemical process under the LMCT excitation was obtained by means of laser flash photolysis.

Prolonged irradiation of $Os^{IV}Cl_6^{2-}$ at 365 nm (Fig. 4b) results in the disappearance of the band with the maximum at 352 nm accompanied by precipitation. The colloid precipitate could be either Os(III) or Os(II) oxide (Os_2O_3 or OsO), or their mixture.

3.2. Laser flash photolysis of $Os^{IV}Cl_6^{2-}$ in the LMCT band region

The results of laser flash photolysis experiments in the time region up to 50 μs with excitation at 355 nm are shown in Fig. 5.

Kinetic curves (Fig. 5a) could be fitted by an exponential function, but the characteristic time is wavelength-dependent. Fig. 5b shows the intermediate absorption spectrum at different time delays. The amplitude of intermediate absorption was linear *vs.* laser pulse energy (Fig. S3 of the ESI†), which allowed us to rule out the possibility of two-photon processes initiated by the laser excitation.

One can see that the absorption in the region 520–750 nm with the maxima around 590 and 710 nm decays faster than the absorption in the other spectral regions. The characteristic time of this faster decay (see *e.g.* the kinetic curve corresponding to 610 nm in Fig. 5a) is about 7 μs (6.7 ± 0.5 μs for the curve corresponding to 610 nm in Fig. 5a).

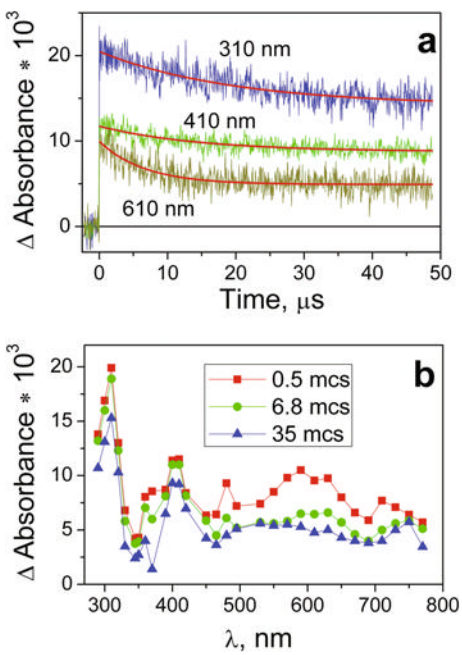

Fig. 5 Laser flash photolysis (355 nm) of $Os^{IV}Cl_6^{2-}$ in ethanol (1.3 × 10^{-4} M, 1 cm cell, air-saturated solution). (a) Examples of kinetic curves with 1-exponential fit (see text). (b) Intermediate absorption spectra at different time delays between excitation and probing.

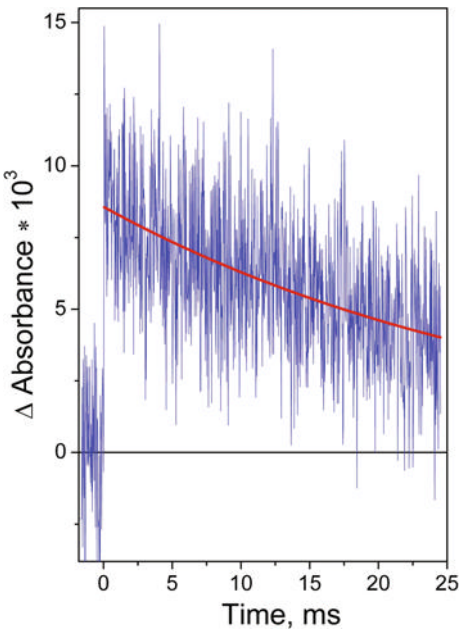

Fig. 6 An example of a kinetic curve obtained by laser flash photolysis (355 nm) of $Os^{IV}Cl_6^{2-}$ in ethanol (1.3 × 10^{-4} M, 1 cm cell, air-saturated solution). Detection at 389 nm. The red curve is the result of an exponential fit.

The complete decay of intermediate absorption occurs in the millisecond time domain. Fig. 6 shows a typical kinetic curve. The characteristic time of the longer process is 32 ± 2 ms.

Therefore, we observed at least two intermediates of Os(III). Furthermore, our attempts to identify the intermediates using quantum chemical calculations of their UV-Vis absorption spectra will be described.

3.3. Photophysical processes followed by 400 nm excitation of $Os^{IV}Cl_6^{2-}$

Experiments on ultrafast pump–probe spectroscopy (transient absorption, TA) were performed with excitation at 400 nm corresponding to the intersection of the two charge transfer bands (Fig. 1 and Fig. S1 of the ESI†). Both transitions are spin allowed, and therefore the immediately formed Frank–Condon (FC) state is the spin triplet. Furthermore, we will mark this FC state as ^{3}(LMCT).

The intermediate absorption spectra were recorded in the wavelength range of 440–680 nm. The time evolution of the intermediate absorption spectrum and typical kinetic curves are shown in Fig. 7. Intermediate absorption appears as a wide band with the maximum in the range of 460 nm; no dramatic changes in the shape of this band occur till its complete disappearance (*ca.* 100 ps). The experimental points corresponding to time delays (−500 fs) < τ < (500 fs) were omitted

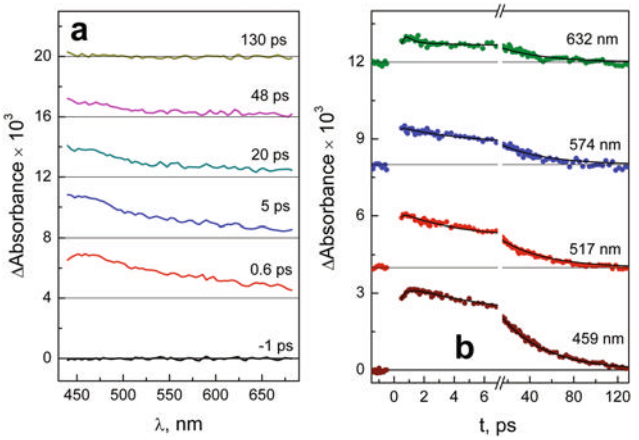

Fig. 7 Results of ultrafast pump–probe experiments (λ_{pump} = 400 nm) with $Os^{IV}Cl_6^{2-}$ (2.3 × 10^{-4} M) in EtOH solution. (a) Intermediate absorption spectra at different time delays between pump and probe pulses. (b) Examples of experimental kinetic curves (dots) and the best three-exponential global fits (solid lines).

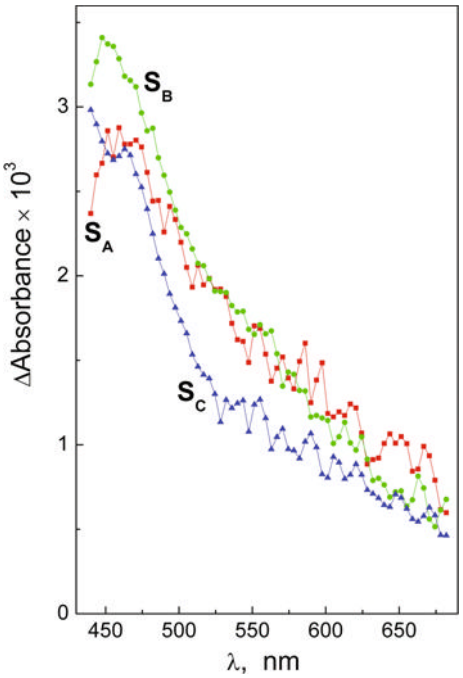

Fig. 8 Results of the ultrafast kinetic spectroscopy experiment (λ_{pump} = 400 nm) with $Os^{IV}Cl_6^{2-}$ (2.3 × 10^{-4} M) in EtOH solution. Species-associated difference spectra (SADS) obtained from the three-exponential global fit (eqn (9)) of experimental kinetic curves and formulae (10)–(12).

because they were affected by the so-called coherent artifact caused by the coherent interactions between pump and probe pulses.[45] Therefore, the early processes occurring immediately after absorption of a light quantum are not accessible for investigation. The only trace of the early processes is the partial increase in absorption in the region of 440–490 nm (see the curve at 459 nm in Fig. 6b) with the characteristic time of *ca.* 0.5 ps.

The whole set of the kinetic curves was globally fitted using a triexponential function (9) (no satisfactory description could be achieved using a biexponential fit).

$$\Delta A(\lambda, t) = A_1(\lambda)e^{-k_1 t} + A_2(\lambda)e^{-k_2 t} + A_3(\lambda)e^{-k_3 t} \quad (9)$$

Treatment of the kinetic curves by means of the triexponential function (9) assumes the sequential decay of the transient absorption A → B → C → (ground state + products). The species-associated difference spectra (SADS) of the individual components were calculated using formulae (10)–(12).[46] The SADS are shown in Fig. 8. The time constants extracted by using the global fit of the kinetic curves are given in Table 2. Note that we do not provide the error for the fastest process (τ_1 = 400 fs). Because of the lack of the experimental points, the calculation error is too high; therefore, the obtained value is considered as an estimation of the lifetime of early processes.

$$S_A(\lambda) = A_1(\lambda) + A_2(\lambda) + A_3(\lambda) \quad (10)$$

$$S_B(\lambda) = A_2(\lambda)\frac{\tau_2 - \tau_1}{\tau_2} + A_3(\lambda)\frac{\tau_3 - \tau_1}{\tau_3} \quad (11)$$

$$S_C(\lambda) = A_3(\lambda)\frac{(\tau_3 - \tau_1)(\tau_3 - \tau_2)}{{\tau_3}^2} \quad (12)$$

The initial transient absorption spectrum appears as a wide band covering all the regions of observation (440–680 nm, SADS S_A in Fig. 8); the maximum lies in the region of 460 nm. Then the differential absorption increases at shorter wavelengths (see the SADS S_B in Fig. 8). The second observed process appears as the narrowing of the absorption band resulting in the formation of the SADS S_C. In the course of the last process the intermediate absorption completely disappears.

The spectral changes occurring after irradiation of $Os^{IV}Cl_6^{2-}$ in ethanol are similar to that in aqueous solutions.[9] Both shapes and lifetimes of the SADS are similar; the main difference is the 1.5 times increase in the lifetime of the last process. Therefore, we can conclude that the observed intermediate corresponding to the SADS S_C is the same as the Key

Table 2 Characteristic lifetimes extracted in ultrafast pump–probe spectroscopy experiment (excitation at 400 nm) with $Os^{IV}Cl_6^{2-}$ in EtOH and the corresponding processes. GS and ^{3}(LMCT) – the ground and initial electronic excited states of $Os^{IV}Cl_6^{2-}$

τ_1, fs	Process	τ_2, ps	Process	τ_3, ps	Process
400[a]	^{3}(LMCT) → $(Os^{IV}Cl_5^-)$*	2.5 ± 1.6	$(Os^{IV}Cl_5^-)$* → $Os^{IV}Cl_5^-$	41 ± 4	$Os^{IV}Cl_5^-$ → GS + products

[a] Estimation.

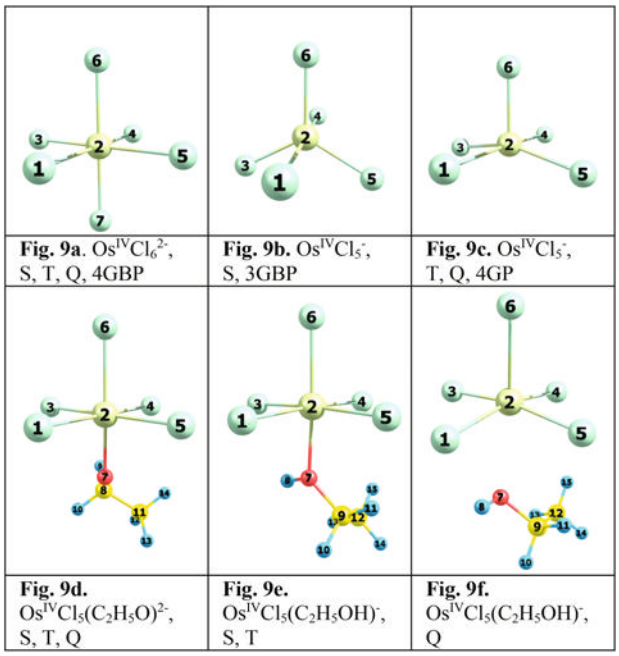

Fig. 9 Optimal geometry of $Os^{IV}Cl_6^{2-}$, $Os^{IV}Cl_5^-$, $Os^{IV}Cl_5(C_2H_5OH)^-$ and $Os^{IV}Cl_5(C_2H_5O)^{2-}$ complexes corresponding to the lowest electronic states with the given multiplicity. Panels **a–f** demonstrate the geometries of the complexes.

Intermediate (KI) observed in aqueous solutions.[9,10] According to the quantum chemical calculation performed in ref. 10, it is either $^3Os^{IV}Cl_5^-$ or $^5Os^{IV}Cl_5^-$ pentacoordinated intermediate having the square pyramidal coordination geometry (Fig. 9).

Consequently, the mechanism of photolysis in the case of d–d band excitation is the same as in the case of aqueous solution. This mechanism is represented by eqn (13)–(17).

$$Os^{IV}Cl_6^{2-}(^3T_{1g}) \xrightarrow{h\nu} {}^3(LMCT)_{hot} \quad (13)$$

$$^3(LMCT)_{hot} \rightarrow \{Os^{IV}Cl_5^-...Cl^-\}^{cage}_{hot} \quad (14)$$

$$^3\{Os^{IV}Cl_5^-...Cl^-\}^{cage}_{hot} \rightarrow \{Os^{IV}Cl_5^-...Cl^-\}^{cage} \quad (15)$$

$$^3\{Os^{IV}Cl_5^-...Cl^-\}^{cage} \rightarrow Os^{IV}Cl_6^{2-}(^3T_{1g}) \quad (16)$$

$$^3\{Os^{IV}Cl_5^- \ldots Cl^-\}^{cage} \xrightarrow{C_2H_5OH} Os^{IV}Cl_5(C_2H_5OH)^- + Cl^- \quad (17)$$

The early processes with the total characteristic time of *ca.* 400 fs are represented by eqn (14). The ^{3}(LMCT) excited state of $Os^{IV}Cl_6^{2-}$ is quickly depopulated to the lowest electronic excited state, which is dissociative. According to ref. 37, this is the $^1T_{2g}$ state. Nevertheless, quantum chemical calculations performed in ref. 10 demonstrated that the lowest electronic excited state of $Os^{IV}Cl_6^{2-}$ is a spin quintet, and this state is dissociative. As a result of dissociation, the $\{Os^{IV}Cl_5^-...Cl^-\}^{cage}$ pair is formed, where $Os^{IV}Cl_5^-$ could be either a spin triplet or a spin quintet (as in the case of aqueous solutions[10]). Because the early processes are hidden by the coherent artifact, we can just say that the SADS S_A corresponds to the superposition of any states formed from the initial ^{3}(LMCT) state, and the first extracted lifetime (τ_1 in Table 2) is an estimation of the real characteristic time of the early processes. The SADS S_B is the spectrum of the vibrationally hot $Os^{IV}Cl_5^-$ complex.

The second observed process with the characteristic time of 2.5 ps is the vibrational cooling of the $\{Os^{IV}Cl_5^-...Cl^-\}^{cage}$ pair, probably superimposed with the translational solvent relaxation. SADS S_C is the spectrum of the $Os^{IV}Cl_5^-$ complex in the ground vibrational state. The last observed process represented by eqn (16) and (17) is the recovery of the ionic pair to the ground state of the initial complex and its transition to the reaction product (with the low probability).

3.4. Results of quantum chemical calculations

The main goal of quantum chemical calculations was to compare the calculated electronic absorption spectra of possible Os(III) intermediates with the experimental spectra obtained by laser flash photolysis (Fig. 5b). To verify the reliability of the calculations, the comparison of the experimental and calculated spectra of the stable species was performed.

The optimized geometric and energetic parameters for the initial $Os^{IV}Cl_6^{2-}$ complex, the intermediate $Os^{IV}Cl_5^-$ complex, the photosolvation product $Os^{IV}Cl_5(C_2H_5OH)^-$, and the possible product of its acid dissociation $Os^{IV}Cl_5(C_2H_5O)^{2-}$ obtained by DFT calculations both in the gas phase and in ethanol are presented in Tables S1–S4 of the ESI.† The influence of the solvent for all the structures was small (±0.02 Å for bond lengths and ±2° for angles). In the case of the $Os^{IV}Cl_5(C_2H_5OH)^-$ complex, the solvent stabilizes the structure. The Os–O(7) bond in the solvent is closer to the covalent bond than in the gas phase (compare lines 1, 3 and 4, 6 in Table S4†).

The optimal structures of the complexes are shown in Fig. 9 (the configuration is indicated as 4GBP – tetragonal bipyramid, 3GBP – trigonal bipyramid, and 4GP – tetragonal pyramid). The results of DFT calculations for $Os^{IV}Cl_6^{2-}$ and $Os^{IV}Cl_5^-$ are in good agreement with those obtained earlier by the Hartree–Fock level of theory using GAMESS-US and FireFly packages,[10,11] which are more time-consuming.

In the case of the initial $Os^{IV}Cl_6^{2-}$ complex, the energy of the lowest triplet state (T) is less than the energies of the lowest singlet (S) and quintet (Q) states (however it should be noted that the energies of T and Q states are close to each other, while the GAMESS-US calculations have resulted in sufficiently lower energy of the T state[10]). Geometries of the S and T states of $Os^{IV}Cl_6^{2-}$ in the gas phase correspond to highly symmetrical 4GBP close to the octahedron (Fig. 9a and Table S1 of the ESI†), while for the Q state a sufficient elongation of bonds corresponding to the axial Cl atoms is observed. A similar elongation is observed for $Os^{IV}Cl_6^{2-}$ in ethanol (Table S1 of the ESI†).

For the pentacoordinated intermediate $Os^{IV}Cl_5^-$, the geometry of the lowest states with the specified multiplicity corresponds to 3GBP for the lowest S state (Fig. 9b) and to 4GP for the lowest T and Q states (Fig. 9c).

Calculation performed for the photosolvation product $Os^{IV}Cl_5(C_2H_5OH)^-$ showed that the S and T states of $Os^{IV}Cl_5^-$ formed stable complexes with an ethanol molecule. In these cases, the geometry of the $Os^{IV}Cl_5^-$ fragment corresponds to 4GP (Fig. 9e), and the Os–O bond length is 2.12 Å, that is the bond is robust. For the Q state of $Os^{IV}Cl_5^-$, the Os–O bond was not formed (Fig. 9f). Note that in the case of $Os^{IV}Cl_5(C_2H_5O)^{2-}$ all the multiplicities are possible (Fig. 9d). In all cases the T state had the lowest energy, but the difference was not large.

The simplest intermediate of Os(III) has a tetracoordinated structure $Os^{III}Cl_4^-$ (Fig. S7 of the ESI†). The quantum-chemical calculations performed in the gas phase and ethanol for doublet and quartet states are presented in Table S5 of the ESI.† Both complexes have square planar configurations. Slight differences of ~0.01 Å manifest themselves in the bond lengths of the complex in the doublet state, while all bond lengths of the complex in the quartet state are the same. The complex in the quartet state is characterized by the lowest energy.

The pentacoordinated intermediate $Os^{III}Cl_5^{2-}$ in both the doublet and quartet states has the geometric structure similar to that of $Os^{IV}Cl_5^-$ in the triplet state. The results presented in Table S6 of the ESI† show that the structure depicted in Fig. 9b is not implemented for the pentacoordinated complex of Os (III). However, there are slight distortions of chlorine's plane for the complex in the quartet state. The Cl(6)–Os–Cl(1,4) bond angles differ from the Cl(6)–Os–Cl(3,5) bond angles. Moreover, the energies of the $^2Os^{III}Cl_5^{2-}$ and $^4Os^{III}Cl_5^{2-}$ complexes are close to each other.

To clarify the geometric and electronic structures of reagents, intermediates and products, the electronic spectra were calculated for complexes of Os(IV) in the triplet state (Fig. 10) and for complexes of Os(III) in both the doublet and quartet states (Fig. 11) (the ground state of the Os(IV) complexes under consideration is triplet, while for the $Os^{III}Cl_5^{2-}$ complex the energies of the doublet and quartet states are close to each other).

The calculated spectra of $Os^{IV}Cl_6^{2-}$ are shifted to the red region relative to the experimental band (Fig. 10a). This is the typical result of the B3LYP calculations for the complexes of platinum group metals.[47] Two intense lines at the top of the panel (Fig. 10a) are in good agreement with the two intense lines at 286 and 358 nm obtained for calculating the gas phase XMCQDPT (10.8)/SBKJC in ref. 10. The occupied and unoccupied orbitals participating in electronic transitions at 392 and 405 nm include the transitions from HOMO−2 to the LUMO and from HOMO−3 plus HOMO−2 to the LUMO, respectively. The LUMO orbital has double degeneracy and consists of the following main atomic orbitals: $d_{xz,xy,yz}(Os)$ and $p_z(Cl_{1,4})$, $p_x(Cl_{6,7})$. The HOMO−2 has triple degeneracy and the following atomic orbitals: the main contributions from $p_{x,y,z}(Cl_{1-7})$ and the minor contributions from $p_{x,y,z}(Os)$. The HOMO−3 has triple degeneracy and the following main atomic orbitals: $p_x(Cl_{3,5,6,7})$, $p_y(Cl_{1,4,6,7})$, $p_z(Cl_{1,3,4,5})$. Comparison with the results of ref. 10 shows that the contributions of the atomic orbitals to the LUMO are similar, while the contributions to

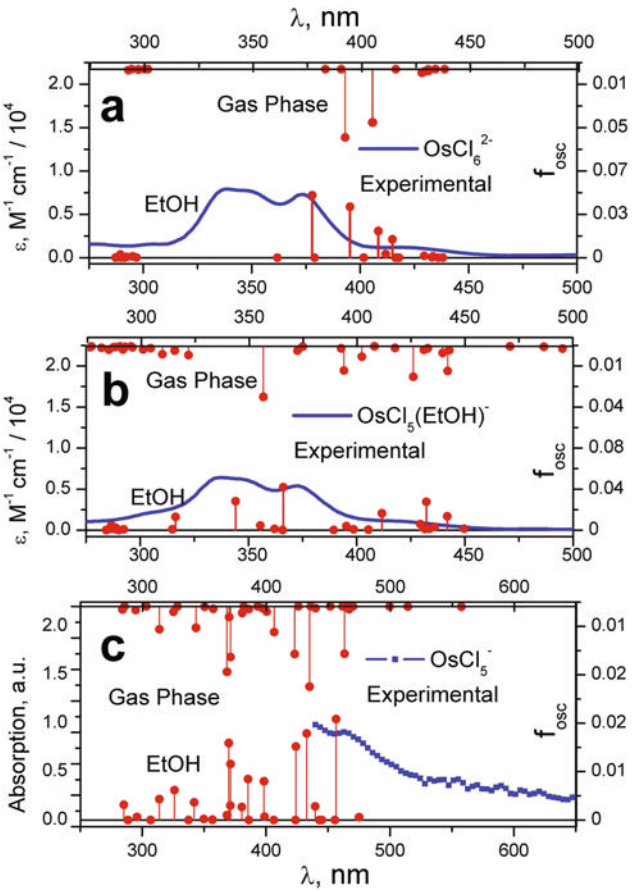

Fig. 10 Experimental (blue lines and dots, solvent – ethanol) and calculated (red dots and vertical lines; top – gas phase; bottom – ethanol solutions) electronic absorption spectra of $Os^{IV}Cl_6^{2-}$ (panel a), $Os^{IV}Cl_5(C_2H_5OH)^-$ (panel b) and $Os^{IV}Cl_5^-$ intermediate (panel c). Left axes – the molar absorption coefficient for experimental spectra of $Os^{IV}Cl_6^{2-}$ and $Os^{IV}Cl_5(C_2H_5OH)^-$, and absorption of the $Os^{IV}Cl_6^{2-}$ intermediate (data of TA experiments represented in arbitrary units). Right axes – the calculated oscillator strengths (top – in the gas phase and bottom – in ethanol). All calculations were performed for the lowest triplet states.

the HOMO and HOMO−2 are different. The nature of the most intense spectral lines is due to the electronic transitions between the ligands and the transition metal. Due to the influence of the solvent, the number of intense lines becomes large, and their positions approach the experimental band.

The calculated spectrum of the photosolvation product $Os^{IV}Cl_5(C_2H_5OH)^-$ is consistent with the experimental one (Fig. 10b). Therefore, the calculated spectra of two stable complexes, $Os^{IV}Cl_6^{2-}$ and $Os^{IV}Cl_5(C_2H_5OH)^-$, are in reasonable agreement with those of the experimental ones. It allowed us to use DFT calculations for modeling the spectra of the possible intermediates.

Fig. 10c shows the calculated spectra of $^3Os^{IV}Cl_5^-$. Note that it is hard to estimate the quality of calculations because of the lack of experimental data at $\lambda < 440$ nm, where calculations predict intense absorption. Definitely, the experimentally observed wing in the region of 500–650 nm is not described by

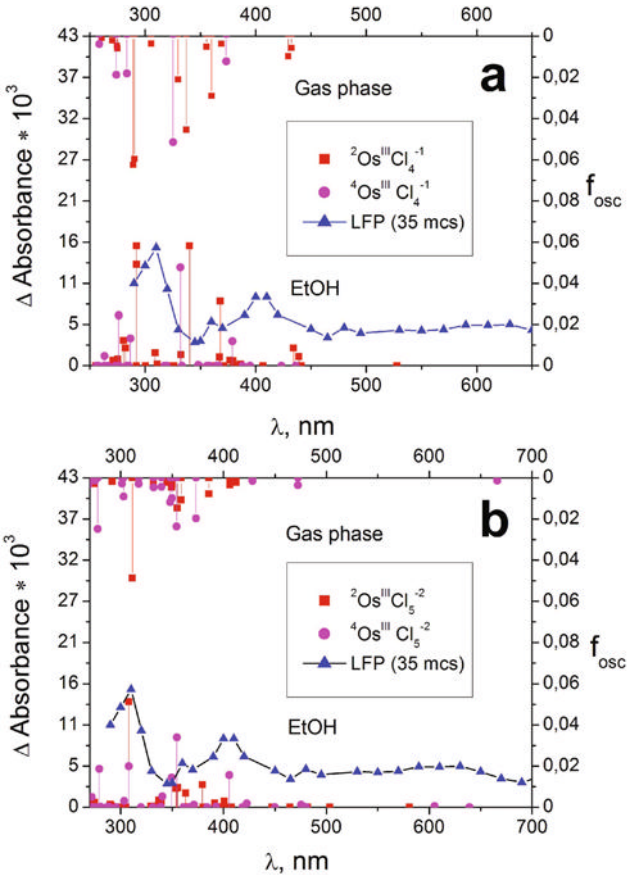

Fig. 11 Experimental and calculated spectra of possible Os(III) intermediates obtained by laser flash photolysis (355 nm) of $Os^{IV}Cl_6^{2-}$ in ethanol. Blue lines and dots represent the spectrum of the intermediate corresponding to the final spectrum in Fig. 5b. Red and magenta dots and lines represent the calculated spectra of $Os^{III}Cl_4^{-}$ (panel a) and $Os^{III}Cl_5^{2-}$ (panel b) complexes (red dots and vertical lines; top – gas phase; bottom – ethanol solutions). Left axes – experimental absorption of the intermediate. Right axes – calculated oscillator strengths (top – in the gas phase and bottom – in ethanol). The calculations were performed for the doublet and quartet states.

calculations. Probably, the reason is that the TD-DFT calculations do not take into account the relativistic effects (spin–orbit coupling).

We checked the possibility to explain the results of the laser flash photolysis experiments (Fig. 5 and 6) by the successive formation of Os(III) intermediates (eqn (5) and (6)). The difference between the shapes of the spectra of the proposed successive Os(III) intermediates was not large (Fig. 5b). Therefore, we calculated the spectra of $Os^{III}Cl_4^{-}$ and $Os^{III}Cl_5^{2-}$ complexes and compared the results with the intermediate absorption measured at 35 μs (which corresponds to the second proposed Os(III) intermediate). The results are shown in Fig. 11.

There is no dramatic difference in the calculated spectra of the doublet and quartet states of both intermediates. Assuming that the probabilities of the doublet and quartet state formation are equal, we can consider the experimental spectrum as the sum of the spectra corresponding to different multiplicities. On the other hand, we can alternatively assume that the transition between two successive Os(III) intermediates with the characteristic time of 7 μs is the intersystem crossing, *e.g.* $^{2}Os^{III}Cl_5^{2-} \rightarrow {}^{4}Os^{III}Cl_5^{2-}$ or vice versa.

One can see (Fig. 11) that the experimental spectrum in the region 290–450 nm could be attributed to both $Os^{III}Cl_4^{-}$ and $Os^{III}Cl_5^{2-}$ complexes (note that the agreement is better for the pentacoordinated intermediate; the calculated maxima of the $Os^{III}Cl_5^{2-}$ absorption at 310 and 405 nm fit well with the experimental spectrum). Calculations for $Os^{III}Cl_5^{2-}$ showed the existence of several lines with a small oscillator strength at 503 nm (0.002), 605 nm (0.151) and 639 nm (0.001) (Fig. 11b, bottom). Because the calculated spectrum of $Os^{III}Cl_4^{-}$ does not cover the region between 500 and 650 nm, it can be assumed that the $^{2,4}Os^{III}Cl_5^{2-}$ complexes make the main contribution to the red wing of the intermediate absorption spectrum detected in the laser flash photolysis experiment (Fig. 5b).

Therefore, the results of the DFT calculations do not contradict the mechanism of photoreduction described by eqn (4)–(6). Additionally, intersystem crossing between the doublet and quartet states of Os(III) intermediates could be one of the stages of the overall photochemical reaction.

The program of quantum chemical calculations was not completed in this work. We did not try to calculate the spectra of the $Os^{III}Cl_{6-n}(C_2H_5OH)^{(3-n)-}$ complexes corresponding to the alternative mechanism described by eqn (7) (the results of calculations performed for $Os^{IV}Cl_5^{-}$ and $Os^{IV}Cl_5(C_2H_5OH)^{-}$ complexes (Fig. 10) showed that the addition of a solvent molecule did not result in dramatic spectral changes). The spectra of possible Os(II) species corresponding to the mechanism described by eqn (8) also were not calculated. More sophisticated calculations are needed to make a choice between the different sets of possible Os(III) intermediates.

4. Conclusions

In this work we examined the primary photophysical and photochemical processes for the $Os^{IV}Cl_6^{2-}$ complex in ethanol. The direction of the photochemical process depends on the nature of the absorption band in which the excitation is carried out. Excitation in the region of the d–d bands results in photosolvation, while excitation in the region of the LMCT band results in the electron transfer from the solvent molecule to the light-excited complex. At least three short-lived Os(IV) and Os(III) intermediates were detected in the time range from tens of femtoseconds to milliseconds. Several reaction mechanics were proposed for the light-induced electron transfer. At least one of the proposed mechanisms does not contradict the quantum chemical calculations of the electronic absorption spectra of the possible intermediates. The more sophisticated calculations of the spectra, which possibly can allow one to make a choice between different mechanisms of photoreduction, are in progress.

Finally, it is well known that the lability of light-induced intermediates makes it possible to use the photochemistry of

metal complexes in the synthesis of both coordination[48] and organic[49] compounds. *e.g.*, Pt(III) intermediates formed by photolysis of $Pt^{IV}Cl_6^{2-}$ in methanol were used to synthesize new Pt(II) complexes with organic ligands.[50–53] In our case, we believe that the lability of photochemically produced Os(IV) and Os(III) intermediates determines the synthetic potential of $OsCl_6^{2-}$ photochemistry in alcohols.

Conflicts of interest

There are no conflicts to declare.

Acknowledgements

The financial support of the Russian Science Foundation (Grant No. 18-13-00246) is gratefully acknowledged.

Notes and references

1 P. A. Lay and W. D. Harman, Recent Advances in Osmium Chemistry, in *Adv. Inorg. Chem*, ed. A. G. Sykes, Academic Press, Inc., Sad Diego, California, 1991, vol. 37, pp. 219–380.
2 D. Kumaresan, K. Shankar, S. Vaidya and R. H. Schmehl, Photochemistry and Photophysics of Coordination Compounds: Osmium, in *Photophysics and Photochemistry of Coordination Compounds II*, ed. V. Balzani and S. Campagna, *Top. Curr. Chem.*, 2007, vol. 281, pp. 101–142, 327 p.
3 E. C. Harvey, B. L. Feringa, J. G. Vos, W. R. Browne and M. T. Pryce, *Coord. Chem. Rev.*, 2015, **282–283**, 77.
4 R. L. Yates, *J. Catal.*, 1982, **78**, 111.
5 Y. Miyake, K. Nakajima, K. Sasaki, R. Saito, H. Nakanishi and Y. Nishibayashi, *Organometallics*, 2009, **28**, 5240.
6 L. A. Pena and P. E. Hoggard, *Photochem. Photobiol.*, 2010, **86**, 467.
7 Von W. Hasenpusch and W. Preetz, *Z. Anorg. Allg. Chem.*, 1977, **432**, 107.
8 E. M. Glebov, V. F. Plyusnin, V. P. Grivin and Yu. V. Ivanov, *Russ. J. Coord. Chem.*, 1997, **23**, 580.
9 E. M. Glebov, I. P. Pozdnyakov, S. G. Matveeva, A. A. Melnikov, S. V. Chekalin, M. V. Rogozina, V. V. Yudanov, V. P. Grivin and V. F. Plyusnin, *Photochem. Photobiol. Sci.*, 2017, **16**, 220.
10 M. V. Rogozina, V. V. Yudanov, R. G. Fedunov, I. P. Pozdnyakov, A. A. Melnikov, S. V. Chekalin and E. M. Glebov, *Photochem. Photobiol. Sci.*, 2018, **17**, 18.
11 M. V. Rogozina, S. G. Matveeva, E. M. Glebov and R. G. Fedunov, *Photochem. Photobiol. Sci.*, 2019, **18**, 1122.
12 I. L. Zheldakov, M. N. Ryazantsev and A. N. Tarnovsky, *J. Phys. Chem. Lett.*, 2011, **2**, 1540.
13 I. L. Zheldakov, *Ultrafast Photophysics and Photochemistry of Hexacoordinated Bromides of Pt(IV), Os(IV), and Ir(IV) in the Condensed Phase Studied by Femtosecond Pump-Probe Spectroscopy*, Ph. D. Thesis, Bowling Green State University, 2010.
14 V. P. Grivin, I. V. Khmelinski, V. F. Plyusnin, I. I. Blinov and K. P. Balashev, *J. Photochem. Photobiol., A*, 1990, **51**, 167.
15 I. P. Pozdnyakov, E. M. Glebov, S. G. Matveeva, V. F. Plyusnin, A. A. Melnikov and S. V. Chekalin, *Russ. Chem. Bull.*, 2015, **64**, 1784.
16 E. M. Glebov, V. F. Plyusnin, N. I. Sorokin, V. P. Grivin, A. B. Venediktov and H. Lemmetyinen, *J. Photochem. Photobiol., A*, 1995, **90**, 31.
17 E. M. Glebov, V. F. Plyusnin, V. P. Grivin, Yu. V. Ivanov, N. V. Tkachenko and H. Lemmetyinen, *Int. J. Chem. Kinet.*, 1998, **30**, 711.
18 C. Rensing, O. T. Ehrler, J.-P. Yang, A.-N. Unterreiner and M. M. Kappes, *J. Chem. Phys.*, 2009, **130**, 234306.
19 E. M. Glebov, A. V. Kolomeets, I. P. Pozdnyakov, V. F. Plyusnin, V. P. Grivin, N. V. Tkachenko and H. Lemmetyinen, *RSC Adv.*, 2012, **2**, 5768.
20 E. M. Glebov, I. P. Pozdnyakov, V. F. Plyusnin and I. Khmelinskii, *J. Photochem. Photobiol., C*, 2015, **24**, 1.
21 S. M. Matveev, D. S. Budkina, I. L. Zheldakov, M. R. Phelan, Ch. M. Hicks and A. N. Tarnovsky, *J. Chem. Phys.*, 2019, **150**, 054302.
22 D. S. Budkina, F. T. Gemeda, S. M. Matveev and A. N. Tarnovsky, *Phys. Chem. Chem. Phys.*, 2020, **22**, 17351.
23 A. A. Melnikov, I. P. Pozdnyakov, S. V. Chekalin and E. M. Glebov, *Mendeleev Commun.*, 2020, **30**, 509.
24 E. M. Glebov, I. P. Pozdnyakov, V. P. Chernetsov, V. P. Grivin, A. B. Venediktov, A. A. Melnikov, S. V. Chekalin and V. F. Plyusnin, *Russ. Chem. Bull.*, 2017, **66**, 418.
25 G. Brauer, *Handbook of Preparative Inorganic Chemistry*, Academic Press, New York, 1965, vol. 2.
26 E. Sosnin, T. Oppenlander and V. Tarasenko, *J. Photochem. Photobiol., C*, 2006, **7**, 145.
27 I. P. Pozdnyakov, V. F. Plyusnin, V. P. Grivin, D. Yu. Vorobyev, N. M. Bazhin and E. Vauthey, *J. Photochem. Photobiol., A*, 2006, **182**, 75.
28 S. V. Chekalin, *Phys. Usp.*, 2006, **49**, 634.
29 N. Tkachenko, *PyG tools for spectroscopy data analysis. User's guide*, 2009, http://butler.cc.tut.fi/~tkatchen/prog/users_guide.pdf.
30 A. D. Becke, *Phys. Rev. A: At., Mol., Opt. Phys.*, 1988, **38**, 3098.
31 C. Lee, W. Yang and R. G. Parr, *Phys. Rev. B: Condens. Matter Mater. Phys.*, 1988, **37**, 785.
32 A. Hellweg, C. Hattig, S. Hofener and W. Klopper, *Theor. Chem. Acc.*, 2007, **117**, 587.
33 D. Andrae, U. Haeussermann, M. Dolg, H. Stoll and H. Preuss, *Theor. Chim. Acta*, 1990, **77**, 123.
34 V. Barone, M. Cossi and J. Tomasi, *J. Chem. Phys.*, 1997, **107**, 3210.
35 M. Cossi, G. Scalmani, N. Rega and V. Barone, *J. Chem. Phys.*, 2002, **117**, 43.
36 J. Tomasi, B. Mennucci and R. Cammi, *Chem. Rev.*, 2005, **105**, 2999.

37 F. Neese, Software update: the ORCA program system, version 4.0, *Wiley Interdiscip. Rev.: Comput. Mol. Sci.*, 2018, **8**, e1327.
38 *Chemcraft – graphical software for visualization of quantum chemistry computations*. https://www.chemcraftprog.com.
39 C. K. Jørgensen, *Mol. Phys.*, 1959, **2**, 309.
40 S. M. Khan, H. H. Patterson and H. Engstrom, *Mol. Phys.*, 1978, **35**, 1623.
41 C. K. Jørgensen and W. Preetz, *Z. Naturforsch.*, 1967, **22a**, 945.
42 V. Balzani and V. Carassiti, *Photochemistry of Coordination Compounds*, Acad. Press, New York, 1970, vol. 257–269, pp. 307–312.
43 L. Moggi, G. Varani, M. F. Manfrin and V. Balzani, *Inorg. Chim. Acta*, 1970, **4**, 335.
44 E. M. Glebov, V. F. Plyusnin, N. V. Tkachenko and H. Lemmetyinen, *Chem. Phys.*, 2000, **257**, 79.
45 L. Palfrey and T. F. Heinz, *J. Opt. Soc. Am. B*, 1985, **2**, 674.
46 A. S. Rury and R. J. Sension, *Chem. Phys.*, 2013, **422**, 220.
47 C. Latouche, D. Skouteris, F. Palazzetti and V. Barone, *J. Chem. Theory Comput.*, 2015, **11**, 3281.
48 O. S. Senturk and F. Ugur, *Synth. React. Inorg. Met.-Org. Chem.*, 2001, **31**, 1843.
49 M. D. Karkas, J. A. Porco Jr. and C. R. J. Stephenson, *Chem. Rev.*, 2016, **116**, 9683.
50 V. P. Grivin, V. F. Plyusnin, I. V. Khmelinski, N. M. Bazhin, M. Mitewa and P. R. Bontchev, *J. Photochem. Photobiol., A*, 1990, **51**, 371.
51 V. P. Grivin, V. F. Plyusnin, I. V. Khmelinski, M. Mitewa and P. R. Bontchev, *J. Photochem. Photobiol., A*, 1991, **62**, 15.
52 V. P. Grivin, V. F. Plyusnin, I. V. Khmelinski, M. Mitewa, J. Angelova, E. Dimitrova and P. R. Bontchev, *J. Photochem. Photobiol., A*, 1992, **63**, 7.
53 V. F. Plyusnin, V. P. Grivin, L. F. Krylova, L. D. Dikanskaya, Yu. V. Ivanov and H. Lemmetyinen, *J. Photochem. Photobiol., A*, 1997, **104**, 45.